SQUID MAGNETOMETERS FOR DEPTH-SELECTIVE, ORIENTED EDDY CURRENT IMAGING

Yu Pei Ma and John P. Wikswo, Jr.

Department of Physics and Astronomy
Vanderbilt University
Box 1807, Station B
Nashville, TN 37235

INTRODUCTION

Because of their unparallelled sensitivity, bandwidth, and spatial resolution, Superconducting Quantum Interference Device (SQUID) magnetometers are unequalled in their ability to image the temporal and spatial variation of weak, low frequency magnetic field . For eddy current NDE, SQUIDs can be used with a low frequency excitation current to image cracks or material loss deep in aluminum structures. To detect the subsurface cracks adjacent to a fastener in multilayer aircraft structures, SQUID NDE measurements have utilized a sheet inducer [1] combined with depth-selective techniques [2, 3], a gridiron coil inducer combined with pulsed eddy current techniques [4], and a double-D inducer [5].

Our approach is to reduce the signal from the rivet and enhance the signal from the crack. Because the phase of the eddy current is a well defined function of depth, the component of the magnetic signal from the eddy current at any desired phase relative to the excitation current provides information about the current distribution at a certain depth below the surface [2, 3]. Since the strength of the signal also depends upon the cross section of the crack or corrosion in the direction of the current, the sensitivity of detection may be optimized by changing the orientation of the excitation current. In addition, the dependence of the amplitude on the current orientation provides information about the geometry of the flaw.

We have used an orthogonal sheet inducer, which can apply an ac magnetic field parallel to the test surface, to induce a large extended eddy current in a desired orientation. We have devised a self-referencing method to determine the geometry of the flaw.

Review of Progress in Quantitative Nondestructive Evaluation, Vol 17
Edited by D.O. Thompson and D.E. Chimenti, Plenum Press, New York, 1998

ORTHOGONAL SHEET INDUCER

The orthogonal sheet inducer has two identical flexible flat cables, each of which has 16 wires connected in series, as shown in Fig. 1. There are two configurations for producing the excitation current:

(A). Two cables carry sinusoidal currents with frequency ω and magnitude I_0 but with a phase difference of 90^o, as shown in Fig. 1a. The resultant current I(t) within the region of overlap has a magnitude I_0 that is time-independent, but with an orientation angle that rotates with the time, $\alpha=\omega t$, with a frequency the same as the frequency of the ac current.

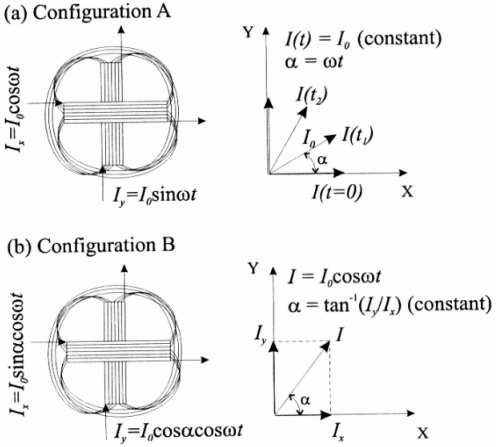

Figure 1. The sketch of the orthogonal sheet inducer. (a) The resultant current has a constant magnitude, but rotates its orientation with a frequency ω. (b) The resultant current is sinusoidal, but has a fixed angle with respect to I_x.

(B). Two cables carry sinusoidal currents with frequency ω in-phase. The magnitudes of the current in each individual cable, I_x and I_y, are determined by the desired angle α of the resultant current, $I_y/I_x=\tan\alpha$, as shown in Fig. 1b. Within the overlap region, the resultant current is also sinusoidal and has the same phase as the current in each individual cable, but is oriented at a fixed angle α with respected to the current in the x direction.

SELF - REFERENCING ANALYSIS

Theoretically, the dipolar signal from a perfect circular hole gives the orientation of the current, so that the direction of the eddy current may be found from the measured field map for a hole. Figure 2 shows the contour maps of a 0.125 inch thick aluminum plate with a 0.5 inch diameter hole and a 0.5 inch long slot, in which the centers are separated by 3 inches. Each cable of the orthogonal inducer carries 35 mA at 500 Hz, but out of phase, so that the resultant excitation current rotates with a frequency of 500 Hz (see configuration *A* in Fig. 1a). Both the in-phase and quadrature components of the SQUID output signal are recorded, which are the images corresponding to the excitation current with angle α=0° and 90°, respectively, so that the images at any desired angle may be obtained. We define 0° current angle as the direction perpendicular to the slot. Since the induced eddy current in the aluminum plate has a phase lag relative to the excitation current, the angle of the eddy current determined by the measured field map is different from the angle of the excitation current. The maps in Fig. 2 are obtained at the angles α of 0° to 160°, which correspond to the eddy current angles of -15° to 145°.

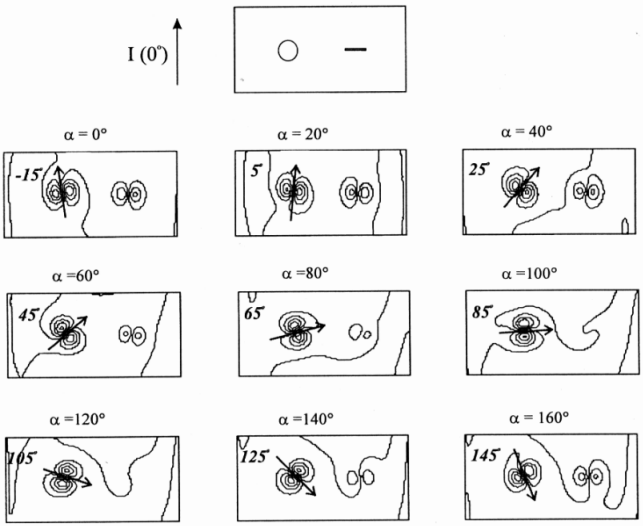

Figure 2. The contour maps of the magnetic signal due to a 0.5 inch diameter circular hole and a 0.5 inch long thin slot using orthogonal sheet inducer with 90° phase difference (configuration *A*). The orientation of the induced eddy current rotates with the same frequency as the frequency of the excitation current, 500 Hz.

There are two major effects when the angle of the excitation current changes: both the orientation of the dipolar signal and its amplitude change. The orientation of the dipole due to the hole rotates with the angle, which implies the orientation of the induced eddy current rotates as indicated by arrows in Fig. 2. The orientation of the dipole due to the slot does not rotate. This is expected because the thin slot does not disturb the current significantly in the direction parallel to the slot. For the hole the amplitude of the dipole does not change with the angle of the current, while the amplitude of the dipole due to the slot varies significantly. The orientation dependence of the amplitude provides us with a self-referencing method to distinguish the signal due to the slot from the signal due to the hole.

To verify the self-referencing method, four samples with oversized flaws were tested: a slot, a hole, a hole combined with one slot, and a hole combined with two slots, as shown in Fig. 3d. All the holes are 0.5 inch diameter, and all the slots are 0.5 inch long. Figure 3a shows the amplitude of the signal at the angles of 0^o to 180^o. The solid line, which is almost constant, is the amplitude of the signal due to the single hole #2. At 90^o the current is parallel to the slots, so that the amplitude of the single slot (dotted line #1) is almost zero, and the amplitudes of the hole-slot combinations are the same as that of the single hole. At 0^o the current is in the direction perpendicular to the slots, so that the amplitude of the signal for the slot reaches a maximum. Here we introduce three parameters: the average amplitude

$$A_{av} = \frac{1}{2}(\max(amplitude) + \min(amplitude)), \tag{1}$$

the amplitude variation

$$\Delta A = \frac{1}{2}(\max(amplitude) - \min(amplitude)), \tag{2}$$

and the asymmetry factor

$$F_{as} = \frac{\Delta A}{A_{av}} \times 100, \tag{3}$$

which is the percentage ratio of the amplitude variation to the average amplitude.

In Fig. 3b, the squares indicate the average amplitude A_{av}, and the error bars indicate the amplitude variation ΔA. The average amplitude is related to the cross sectional area of the flaw, while the amplitude variation depends on the rotational asymmetry of the flaw. Figure 3c is the asymmetry factor F_{as} for the four geometries. The single hole has the lowest F_{as}, and the single slot has the highest. There are several possible reasons that the single hole has a non-zero F_{as} : the imperfect circularity of the hole, the edges of sample or structure nearby, and the error due to the noise. The estimated maximum asymmetry factor associated with the single hole may be used as a threshold, above which there may be a slot in addition to a hole.

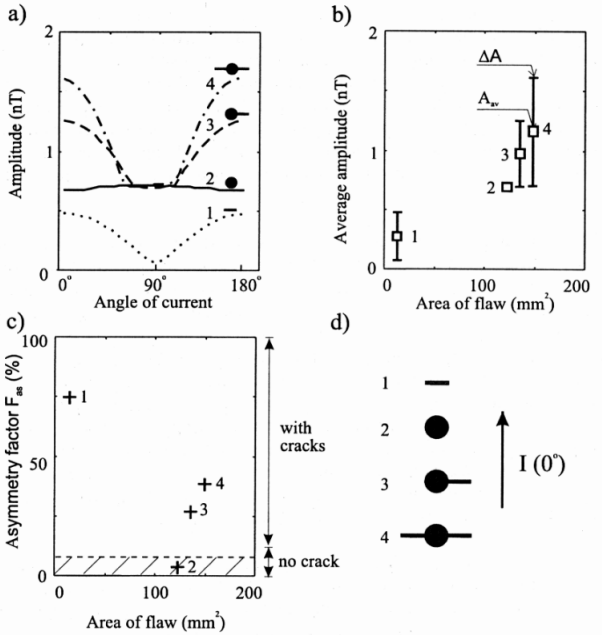

Figure 3. The self-referencing analysis for the four flaws shown at the lower right. (a) The amplitude of the dipolar signal changes with the current orientation, where 0° is defined as the current perpendicular to the slots. (b) The average value of the amplitude over the angles of 0° to 180°. The error bars indicate the amplitude variation. (c) The asymmetry factor F_{as}. The dashed line is a threshold, above which the slots are found.

DEPTH - SELECTIVE AND SELF - REFERENCING METHOD

In our previous papers [2, 3] we have discussed depth-selective techniques for enhancing the signal from the subsurface flaw using the sheet inducer. The phase of the induced eddy current is a function of the depth for a fixed sample at fixed frequency. At a particular phase, the current below the surface is larger than the surface current, so that a subsurface flaw may produce a larger signal than does a surface flaw. In addition, the current at a particular depth changes polarity, so that a flaw at that location produces a quadrupole signal instead of a dipolar signal.

Using the rotating excitation configuration A, shown in Fig. 1a, and a two-phase lock-in amplifier, one measurement provides the pair of images for any desired phase. The phase of the image corresponds to the direction of the excitation current. However, the phase of the induced eddy current changes with depth. Below the surface of the conductor, the rotating angle has a lag with respect to the surface current. Since the image at a particular phase, which is related to a particular angle of the excitation current, is the total contribution of the field due to the eddy current through the thickness of the conductor, the depth information, which is associated with a phase lag, can not be extracted.

For combining the self-reference method with the depth-selective technique, it is better to use configuration B, in which the two cables of the orthogonal inducer carry the current in-phase (see Fig. 1b). The angle of the excitation current α is determined by the ratio of the current in two cables, $\alpha = \tan^{-1}(I_y / I_x)$. The self-referencing method would require a separate measurement for each current direction, which is time consuming. We have shown that the superposition of the eddy current excited by $I_x=I_1$ and $I_y=0$ and the eddy current excited by $I_x=0$ and $I_y=I_2$, is equal to the eddy current excited by simultaneous current $I_x=I_1$ and $I_y=I_2$. In other words, the superposition of the two images, obtained from two separate measurements when the corresponding currents are orthogonal, is equivalent to the image obtained from one measurement with the current angle $\alpha = \tan^{-1}(I_y / I_x)$. We have verified this experimentally. Thus two separate measurements, each of which is obtained by injecting the current through the one cable of the orthogonal inducer, is sufficient for the self-referencing method.

This technique has been tested with a sample provided by Lockheed, as shown in Fig. 4e. The test sample is made of two 0.125 inch thick 7075-T6 aluminum plates bolted together by four 0.25 inch diameter flat-head aluminum fasteners which simulate the rivets. The crack defects beneath the rivet are simulated by 0.25 inch long EDM slots. As shown in Fig. 4e, adjacent to rivet #1 there is a 0.25 inch slot at the second layer, adjacent to rivet #2 there are two slots in both the first and second layers. Beneath rivet #3 is a slot in the first layer, and rivet #4 without any slots is used for reference. The data shown in Fig. 4a are the results from two separate scans using two orthogonal currents I_x and I_y. For each scan, both the in-phase and quadrature signals are recorded. Then for each phase, the magnetic images corresponding to current angles ranging from 0° to 180° are obtained mathematically.

Figure 4 shows the results obtained by combining the depth-selective technique with the self-referencing method. At phase 10°, as shown in Fig. 4a, the amplitude of rivet #1, with the second layer slot, is similar to the reference rivet #4. The amplitude of the rivet #3 with the first layer slot is almost as large as that of the rivet #2 with slots in both layers. This indicates that the main contribution to the signal at phase 10° is from the first layer slot. At phase 95° (see Fig. 4b) the amplitude of rivet #1 with second layer slot becomes as large as that of rivet #2 with slots in both layers, which are much larger than that of rivet #3 with the first layer slot. This implies that the second layer slots dominate at phase 95°.

The asymmetry factors F_{as} at phase 10° and 95° are shown in Fig. 4c and 4d, respectively. The maximum F_{as}, obtained in the phase from 0° to 180° for the reference rivet #4, is 20% and is chosen as a threshold indicated by the dashed line. The asymmetry factor of rivet #1 with the second layer slot is below the threshold at phase 10° (see Fig. 4c), however, it is well above the threshold at phase 95°. The larger asymmetry factor of the reference rivet #4 may be due to the misalignment of the rivet.

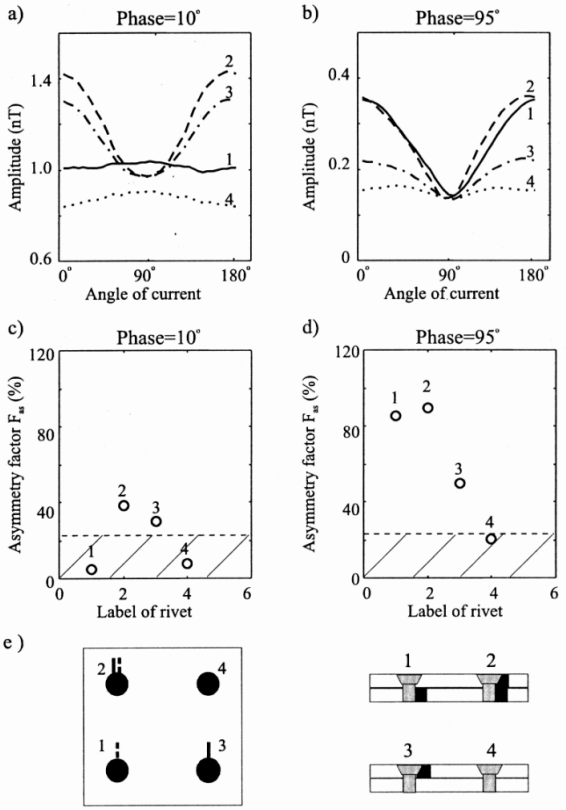

Figure 4. Depth-selective self-referencing method using orthogonal sheet inducer. (a) The amplitude at phase 10°. (b) The amplitude at phase 95°. In both (a) and (b), the solid line is for rivet #1 with the second layer slot, the dashed line is for rivet #2 with slots at both layers, the dash-dotted line is for rivet #3 with the first layer slot, and the dotted line is for reference rivet #4. (c) The asymmetry factor at phase 10°. (d) The asymmetry factor at phase 95°. (e) The sketch of the Lockheed test sample.

CONCLUSIONS

The self-referencing method can identify the asymmetric geometry of the flaw or inclusion without visualization and reference standard. Combining the depth-selective techniques with the self-referencing method, we are able to extract the signal of the second layer cracks from the large signal due to the rivets. This technique may be applied to aircraft NDE, especially for inspection of the cracks beneath the rivets in lap joint structures. Since this method provides a threshold without visual inspection, it may be useful for an automated inspection system.

ACNOWLEDGMENTS

We wish to thank Anthony Ewing for his comments on the manuscript. This work is supported by AFOSR Grant F49620-93-0268.

REFERENCE

1. Y.P. Ma and J. P. Wikswo, Jr., in *Review of Progress in QNDE*, Vol. 13, D.O. Thompson and D.E. Chimenti, Eds., New York: Plenum Press, pp. 303-309, (1994).
2. Y.P. Ma and J.P. Wikswo, Jr., *J. of Nondestructive Evaluation*, Vol.14, No.3, (1995).
3. Y.P. Ma and J. P. Wikswo, Jr., in *Review of Progress in QNDE*, Vol. 15, D.O. Thompson and D.E. Chimenti, Eds., New York: Plenum Press, pp. 401-408, (1996).
4. W. Podney and J Moulder, in *Review of Progress in QNDE*, Vol. 16, D.O. Thompson and D.E. Chimenti, Eds., New York: Plenum Press, pp. 1037-1044, (1997).
5. H.-J. Krause, R. Hohmann, H. Soltner, D. Lomparski, M. Gruneklee, M, Banzet, J. Schubert, W. Zander, Y. Zhang, W. Wolf, H. Bousack, A.I. Braginski,M.L. Lucia, E. Zimmermann, G. Brandenburg, U. Clemens, H. Rongen, H. Halling, M.I. Faley, U. Poppe, H. Buschmann, G. Sporl, A. Binneberg, and M. Junger, in *Review of Progress in QNDE*, Vol. 16, D.O. Thompson and D.E. Chimenti, Eds., New York: Plenum Press, pp. 1053-1060, (1997).